MATERIALS RESEARCH SOCIETY SYMPOSIUM PROCEEDINGS VOLUME 233

Synthesis/Characterization and Novel Applications of Molecular Sieve Materials

Symposium held May 1-3, 1991, Anaheim, California, U.S.A.

EDITORS:

Robert L. Bedard
UOP, Tarrytown, New York, U.S.A.

Thomas Bein
Purdue University, West Lafayette, Indiana, U.S.A.

Mark E. Davis
California Institute of Technology, Pasadena, California, U.S.A.

Juan Garces
Dow Chemical Company, Midland, Michigan, U.S.A.

Victor A. Maroni
Argonne National Laboratory, Argonne, Illinois, U.S.A.

Galen D. Stucky
University of California at Santa Barbara, Santa Barbara, California, U.S.A.

MRS MATERIALS RESEARCH SOCIETY
Pittsburgh, Pennsylvania

1991

Contents

*Invited Paper

*Invited Paper

*Invited Paper

DOPING AND BAND-GAP ENGINEERING OF AN INTRAZEOLITE TUNGSTEN(VI) OXIDE SUPRALATTICE

Geoffrey A. Ozin[a], Andrzej Malek[a], Richard Prokopowicz[a], Peter M. Macdonald[a], Saim Özkar[b], Karin Moller[c] and Thomas Bein[c].
[a]Lash Miller Chemistry Laboratories, University of Toronto, 80 St. George Street, Toronto, Ontario, Canada M5S 1A1
[b]Chemistry Department, Middle East Technical University, Ankara, Turkey.
[c]Department of Chemistry, University of New Mexico, Albuquerque, NM, 87131, USA

ABSTRACT

New results are presented concerning the topotactic self-assembly, n-type doping and band-gap engineering of an intrazeolite tungsten(VI) oxide supralattice $n(WO_3)$-$Na_{56}Y$, where $0 < n \leqslant 32$, built-up of single size and shape $(WO_3)_2$ dimers. In particular it has been found that the oxygen content of these dimers can be quantitatively adjusted by means of a thermal vacuum induced reversible reductive-elimination oxidative-addition of dioxygen. This provides access to new $n(WO_{3-x})$-$Na_{56}Y$ materials ($0 < x \leqslant 1.0$) in which the oxygen content, structural properties and electronic architecture of the dimers are changed. In this way one can precisely control the oxidation state, degree of n-doping and band-filling of a tungsten(VI) oxide supralattice through an approach which can be considered akin to, but distinct in detail to, that found in the Magneli crystallographic shear phases of non-stoichiometric bulk WO_{3-x}. Another discovery concerns the ability to alter local electrostatic fields experienced by the tungsten(VI) oxide moieties housed in the 13Å supercages of $16(WO_3)$-$M_{56}Y$, by varying the ionic potential of the constituent supercage M^+ cations across the alkali metal series. This method provides the first opportunity to fine-tune the band-gap of a tungsten(VI) oxide supralattice. A miniband electronic description is advanced as a qualitative first attempt to understand the origin of the above effects. The implications of these discoveries are that cluster size, composition and intrinsic electrostatic field effects can be used to "chemically manipulate" (engineer) the doping and band architecture of intrazeolite supralattices of possible interest in quantum electronics and nonlinear optics.

Introduction

The photo-oxidation of α-cage encapsulated $n\{W(CO)_6\}$-$Na_{56}Y$, provides a mild, clean and quantitative synthetic pathway to single size and shape tungsten(VI) oxide clusters $n(WO_3)$-$Na_{56}Y$ according to the reaction [1]:

$$n\{W(CO)_6\}\text{-}Na_{56}Y + 9n/2O_2 \xrightarrow{h\nu} n(WO_3)\text{-}Na_{56}Y + 6nCO_2$$

A combination of spectroscopy, diffraction and microscopy probes, including EXAFS structure analysis [2] demonstrates that over the entire $W(CO)_6$ loading

range $0 < n \lesssim 32$, achieved via the sequential saturation impregnation-photooxidation process:

$$
\begin{array}{lll}
16\{W(CO)_6\}\text{-}Na_{56}Y & \text{--->} & 16(WO_3)\text{-}Na_{56}Y \\
8\{W(CO)_6\},\ 16(WO_3)\text{-}Na_{56}Y & \text{--->} & 24(WO_3)\text{-}Na_{56}Y \\
4\{W(CO)_6\},\ 24(WO_3)\text{-}Na_{56}Y & \text{--->} & 28(WO_3)\text{-}Na_{56}Y \\
\vdots & & \vdots \\
1\{W(CO)_6\},\ 30(WO_3)\text{-}Na_{56}Y & \text{--->---><---} & 32(WO_3)\text{-}Na_{56}Y
\end{array}
$$

only the population of the $(WO_3)_2$ dimer building block grows within the zeolite Y host lattice to form a $8(WO_3)_2$-$Na_{56}Y$ supralattice of dimers at half-loading n=16, and eventually to a $8\{(WO_3)_2\}_2$-$Na_{56}Y$ supralattice of dimers-of-dimers (rather than $(WO_3)_4$ tetramers) at saturation-filling n=32, as illustrated in Figure 1.

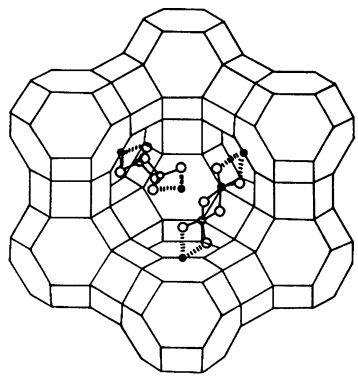

1. Chem-X space filling model for two $(WO_3)_2$ dimers anchored to the $4Na^+$ site II cations in the α-cage of $Na_{56}Y$, (2c).

In this summary paper we report for the first time simple chemical means of injecting variable numbers of electrons into, and adjusting the magnitude of the electrostatic fields experienced by the tungsten(VI) oxide moieties in zeolite Y.

Results And Discussion

A) Doping

Temperature programmed thermal treatment of $n(WO_3)$-$Na_{56}Y$ ($0 < n \lesssim 32$) shows that dioxygen loss begins around 200°C to yield beautiful royal blue ($0 < n \lesssim 8$) or metallic blue-grey ($8 \lesssim n \lesssim 32$) or metallic grey ($n \approx 32$) materials with W:O = 1:2.5 at 300°C. Further dioxygen evolution continues between 300-400°C to eventually yield homogeneous white materials with W:O = 1:2. This

process can be quantitatively reversed in O_2 at 300°C, recreating the original material $n(WO_3)$-$Na_{56}Y$ but by-passing the intermediate phase $n(WO_{2.5})$-$Na_{56}Y$. These observations provide compelling evidence for the reductive-elimination oxidative-addition sequence of reactions:

$$n(WO_3)\text{-}Na_{56}Y \xrightarrow[VAC]{300^\circ C} n(WO_{3-x})\text{-}Na_{56}Y \xrightarrow[VAC]{400^\circ C} n(WO_2)\text{-}Na_{56}Y$$

$$n(WO_2)\text{-}Na_{56}Y \xrightarrow{300^\circ C;\ O_2} n(WO_3)\text{-}Na_{56}Y$$

A combination of PXRD, $^{29}Si/^{27}Al/^{23}Na$ MAS-NMR, Raman, Na^+ cation Far-IR and νOH_α Mid-IR experiments performed on a range of $n(WO_{3-x})$-$Na_{56}Y$ samples demonstrate that just like the parent material $n(WO_3)$-$Na_{56}Y$, the degree of crystallinity and integrity of the framework of the zeolite Y host material is maintained, little alteration in the host unit cell dimension is observed (around 24.69 Å for all samples), no bulk WO_{3-x} oxides are detected, and the WO_{3-x} guests remain internally confined and homogeneously dispersed throughout the α-cages of the host.

The optical reflectance spectra provide some interesting structure-electronic clues about the constitution of these materials. From inspection of some representative data for $n(WO_{3-x})$-$Na_{56}Y$ shown in Figure 2,

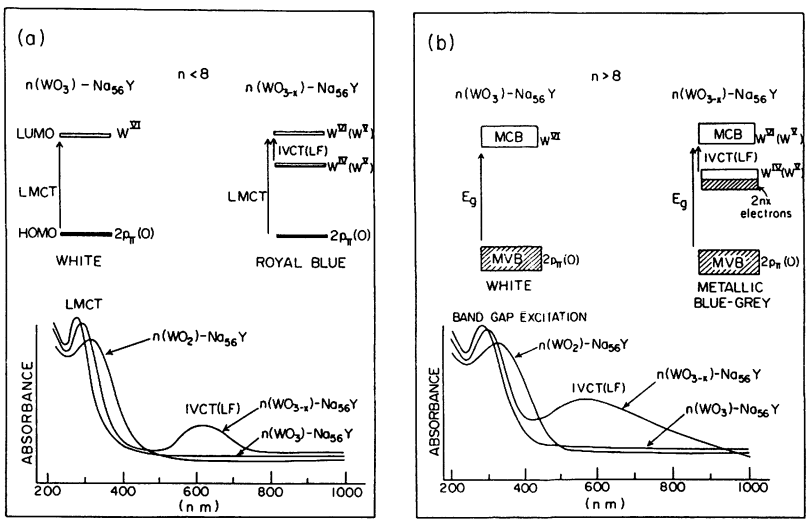

2. UV-visible reflectance spectra of $n(WO_{3-x})$-$Na_{56}Y$ for $n < 8$ and $n > 8$, where $x = 0, 0.5, 1$.

one spots two informative effects. An intense broad "blue" visible-band and a

red-shifted uv-band is observed on passing from $n(WO_3)$-$Na_{56}Y$ to $n(WO_{2.5})$-$Na_{56}Y$. This blue band broadens and the uv-band red shifts on passing from "isolated" ($n \lesssim 8$) to "coupled" ($8 \lesssim n \lesssim 32$) $WO_{2.5}$ materials. The blue band disappears and the uv-band-shifts even further on passing from $n(WO_{2.5})$-$Na_{56}Y$ to $n(WO_2)$-$Na_{56}Y$. The uv-band red-shifts again on passing from "isolated" ($n \lesssim 8$) to "coupled" ($8 \lesssim n \lesssim 32$) WO_2 materials, Figure 2.

Recall (1) that the parents $n(WO_3)$-$Na_{56}Y$ display an $O^{-II}(2p\pi) \dashrightarrow W^{VI}(5d)$ absorption edge around E_g = 3.1-3.5 eV (computer fit, Kubelka Munk, $\alpha^{da}=K(E-E_g)^{1/2}$) which is assigned to an interstate (HOMO-LUMO) LMCT excitation for the "isolated" $(WO_3)_2$ dimers ($n \lesssim 8$), Figure 3 and an interminiband (MVB-MCB) transition for the "coupled" $(WO_3)_2$ dimers ($8 \lesssim n \lesssim 32$), Figure 3.

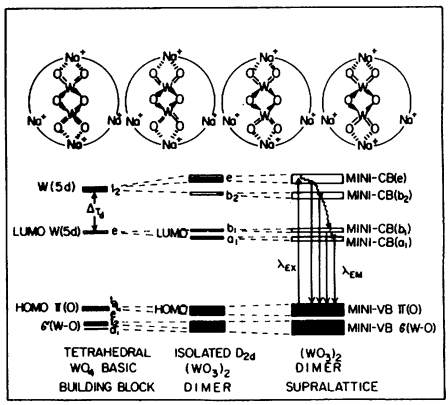

3. Evolution of a qualitative miniband electronic scheme for a $(WO_3)_2$ dimer superalattice, $16(WO_3)$-$Na_{56}Y$.

Some of the xenon lamp and laser induced emission/excitation spectra with time resolution obtained for $n(WO_3)$-$Na_{56}Y$ are depicted in Figure 4. The observation of considerable structure under the absorption-edge (450, 400, 374 nm excitation spectra), short (μs, 450-300 nm) and long (ms, 680-500 nm) lifetime emissions, alerts one to the existence of complex coupling architecture in the MCB, possible "excitonic" emissions close to the miniband-gap energy, as well as "forbidden or trap" emissive states (Figure 4).

With the above information, the "blue" band in $n(WO_{2.5})$-$Na_{56}Y$ ($n \lesssim 8$) can be assigned to either a W(IV) → W(VI) intervalence-charge-transfer (IVCT) or a W(V) → W(V) ligand-field (LF) transition while the uv-band is ascribed to either a O(-II) → W(VI) or O(-II) → W(V) LMCT transition (3) (Figure 2). Where the clusters in $n(WO_{2.5})$-$Na_{56}Y$ first begin to couple (through space or zeolite framework) these IVCT (LF) and LMCT bands appear to broaden and/or red-shift. The IVCT (LF) band disappears in $n(WO_2)$-$Na_{56}Y$ ($n \lesssim 8$) with concomitant red-shifting of the O(-II) → W(IV) LMCT band. Similar shifting and broadening effects occur in $n(WO_2)$-$Na_{56}Y$ at $n \gtrsim 8$. Note that all $n(WO_{3-x})$-$Na_{56}Y$ samples

(300-77K) are EPR silent but all yield high quality $^{29}Si/^{27}Al/^{23}Na$ MAS-NMR spectra (see later).

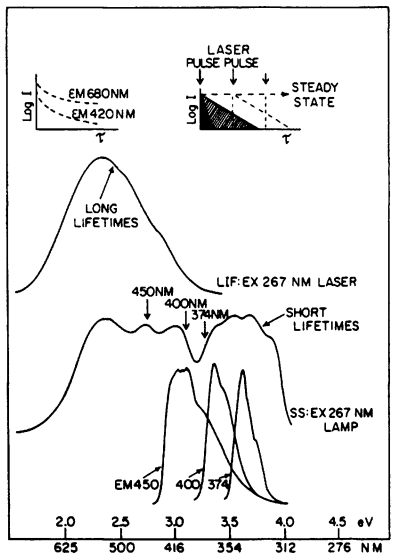

4. Selected photophysical properties of $16(WO_3)$-$Na_{56}Y$

Adsorption-induced ^{23}Na MAS-NMR chemical shifts and Far-IR Na^+ translatory mode frequency shifts provide direct and complimentary evidence for the anchoring of WO_{3-x} moieties to α-cage Na^+ cations in all three samples $n(WO_{3-x})$-$Na_{56}Y$ (x = 0, 0.5, 1). Representative ^{23}Na MAS-NMR data which illustrate this point are shown in Figure 5.

In fully dehydrated $Na_{56}Y$ one observes an intense asymmetric ^{23}Na resonance at -12 ppm which arises from a convolution of signals due to Na^+ cations mainly in sites II, I, I' (2b). The most prominent narrow component centred at -12 ppm is ascribed to Na_I^+ (six coordinate, hexagonal prism, essentially O_h symmetry, smallest second order quadrupole broadening). All other hexagonal six-ring $Na^+_{II,I'}$ (α, β-cage respectively) have lower symmetries C_{3v}, are expected to exhibit more pronounced second order quadrupole broadening, and appear to fall within the high-field shoulder (-22 and -38 ppm) of the main ^{23}Na resonance, Figure 5. In $16(WO_3)$-$Na_{56}Y$, the $(WO_3)_2$ dimer perturbs one of the components of the $Na_{56}Y$ high field shoulder around -22 ppm with a corresponding increase in its intensity (Figure 5). Similar effects exist in the ^{23}Na MAS-NMR spectra of both $16(WO_{2.5})$-$Na_{56}Y$ and $16(WO_2)$-$Na_{56}Y$, where one notes that the perturbed ^{23}Na resonance is broader and less well pronounced in $16(WO_{2.5})$-$Na_{56}Y$ compared to $16(WO_2)$-$Na_{56}Y$ and $16(WO_3)$-$Na_{56}Y$ (Figure 5). Adsorption induced charge transfer to the terminal tungsten dioxo group of the imbibed WO_{3-x} moieties from the Na^+_{II} cations in $Na_{56}Y$ will serve to (a) decrease the shielding (b) lower the

second order quadrupole broadening (c) reduce electric field gradients and (d) cut-down or eliminate site-exchange processes of those Na^+ cations accessible to the act of anchoring. The primary effects of anchoring are then expected to be a shift of the α-cage $^{23}Na_{II}$ NMR resonance to lower fields with a concomitant enhancement of its intensity with increasing symmetry around the Na^+_{II} site, Figure 5. This appears to describe the overall state-of-affairs for the series $16(WO_{3-x})$-$Na_{56}Y$ where in essence one "discovers" Na^+_{II} through its selective anchoring and "locking" onto the WO_{3-x} moieties, Figure 5.

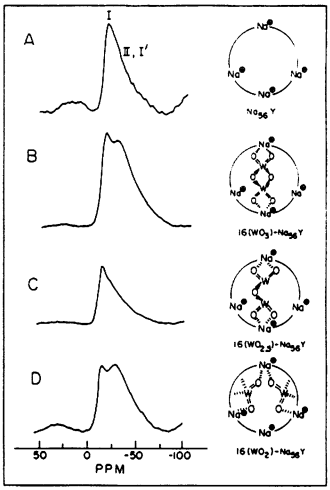

5. ^{23}Na MAS-NMR data for A) $Na_{56}Y$ B) $16(WO_3)$-$Na_{56}Y$ C) $16(WO_{2.5})$-$Na_{56}Y$ and D) $16(WO_2)$-$Na_{56}Y$

^{23}Na DOR-NMR studies are underway to explore these systems more thoroughly [4].

EXAFS structure analysis has been successfully applied to the precursor $8\{W(CO)_6\}$-$Na_{56}Y$, photo-oxidation products $16(WO_3)$-$Na_{56}Y$, $28(WO_3)$-$Na_{56}Y$, $32(WO_3)$-$Na_{56}Y$ and thermal reductive-elimination products $16(WO_{2.5})$-$Na_{56}Y$, $32(WO_{2.5})$-$Na_{56}Y$, $16(WO_2)$-$Na_{56}Y$, $28(WO_2)$-$Na_{56}Y$ and $32(WO_2)$-$Na56_Y$ (2c, 3). A summary of these experiments is shown in Figure 6. For the precursor, the EXAFS data confirm that the $W(CO)_6$ guest maintains its structural integrity with virtually no observable perturbations of the skeletal W-C≡O, R = 2.06 Å (2.058 Å), N_c = 6.5(6.0), and ligand W-C≡Ω, R = 3.21 Å (3.206 Å), N_o = 6.8(6.0) bonds compared to those found for the same molecule in the free state (numbers in parenthesis). Estimates of uncertainty in reported R and N values are ± 0.02 Å and ± 20% respectively. The EXAFS structure analysis results for the photo-oxidation products $16(WO_3)$-$Na_{56}Y$, $28(WO_3)$-$Na_{56}Y$ and $32(WO_3)$-$Na_{56}Y$ are very similar, and display the presence of two short terminal W=O bonds (1.75 - 1.78 Å) and two long bridging W-O bonds (1.94 - 1.96 Å), together with a short distance to a second W (3.24 - 3.31 Å). This bond-length and coordination number information for n = 16, 28 and 32 samples is interpreted in terms of the

formation of a "single kind" of tungsten(VI) trioxide dimer unit $(WO_3)_2$, most likely interacting with Na^+_{II} cations (Far-IR/NMR) as shown in Figure 6. All the data for $16(WO_3)$-$Na_{56}Y$ support the contention of a uniform array of single-size and shape $(WO_3)_2$ dimers housed in the 13 Å supercages of the zeolite Y host. The sequential addition of WO_3 units to the $16(WO_3)$-$Na_{56}Y$ sample to eventually form "fully" filled $32(WO_3)$-$Na_{56}Y$ appears to increase the $(WO_3)_2$ dimer population, causing a build-up of α-cage dimers-of-dimers $\{(WO_3)_2\}_2$ (Figure 1),

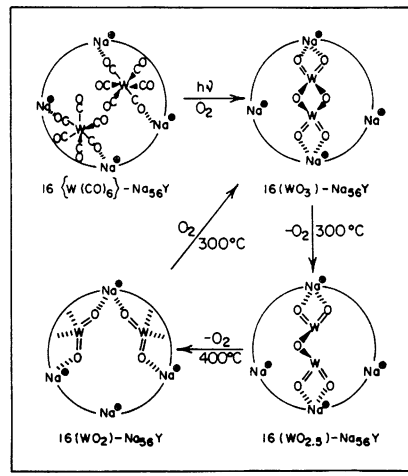

6. Summary of structures and anchoring schemes for α-cage encapsulated precursor $16\{W(CO)_6\}$-$Na_{56}Y$ as well as its photo-oxidation product $16(WO_3)$-$Na_{56}Y$ and corresponding reductive-elimination, oxidation-addition products $16(WO_{3-x})$-$Na_{56}Y$.

rather than further cluster growth to trimers $(WO_3)_3$ and/or tetramers $(WO_3)_4$.

The presently observed EXAFS data set for the $16(WO_{2.5})$-$Na_{56}Y$ sample was not of sufficient quality (5) to permit reliable determination of the oxygen distances or coordination numbers. However, it is valid to make the qualitative statement that W-W backscattering was observed, hence leading to the conclusion that the tungsten oxide moiety in this case is at least dimeric, like that found in $16(WO_3)$-$Na_{56}Y$. Interestingly the EXAFS data of the $32(WO_{2.5})$-$Na_{56}Y$ sample are very similar to those of its parent $32(WO_3)$-$Na_{56}Y$ showing two kinds of short/long W=O/W-O (1.75 - 1.95 Å) bond, but now signals a short distance to three other W(3.30 Å). The bond lengths and coordination numbers for both types of oxygen and tungsten, are fully consistent with a "tetrameric" structure wherein the four tungsten atoms lie at the apices of a tetrahedron. The EPR silence of the $16(WO_{2.5})$-$Na_{56}Y$ dimer implies the existence of either a spin-paired singlet or a rapidly relaxing triplet electronic configuration for the two possible dimer formulations, namely either single valent $ZONa...O_2W(V)(\mu\text{-}O)W(V)O_2...NaOZ$ or mixed valence $ZONa...O_2W(IV)(\mu\text{-}O)W(VI)O_2...NaOZ$. The ability to collect

high quality ^{29}Si, ^{29}Al, ^{23}Na MAS-NMR spectra for this sample favours the former spun paired diamagnetic assignment. Much more work, in particular XPS, is needed to clarify this fascinating point.

The EXAFS data of the $16(WO_2)$-$Na_{56}Y$ material are quite distinct to that of the other two samples, indicating only one W-O shell with R = 1.81 Å N_o = 4.1 which is very similar to that of the Na_2WO_4 reference compound. There is no evidence of W-W backscattering in the $16(WO_2)$-$Na_{56}Y$ material. The EXAFS results for $28(WO_2)$-$Na_{56}Y$ and $32(WO_2)$-$Na_{56}Y$ are essentially identical to those of $16(WO_2)$-$Na_{56}Y$. The best model for these intrazeolite WO_2 materials is a 4-ring oxygen framework coordination site to the tungsten(IV) centre of a low spin monomeric WO_2 moiety, of which the terminal W=O oxygens interact with Na^+_{II} as indicated in Figure 6. This is the best way to reconcile the oxygen coordination number, tungsten(IV) oxidation state and Na^+ anchoring interaction clues for $n(WO_2)$-$Na_{56}Y$ (where n = 16, 28, 32) obtained from EXAFS, UV-VIS, FAR-IR, EPR and MAS-NMR spectroscopies.

B) Band-Gap Engineering

The feasibility of fine-tuning the band-gap of the $16(WO_3)$-$M_{56}Y$ supralattice is illustrated in Figure 7. On moving from M = H to Cs at the two extremes one observes a blue-shift of the absorption edge (computer fit, Kubelka Munk, $\alpha^{da} = K(E-E_g)^{1/2}$) of about 0.75 eV. E_g values estimated in this way are H(3.10 eV), Li(3.53 eV), Na(3.33 eV), K(3.74 eV), Rb(3.85 eV), Cs(3.85 eV). Assuming the $(WO_3)_2$ dimer structure is maintained across the series M = H, Li, Na, K, Rb, Cs, one can envisage that enhanced local electrostatic fields arising from the presence of M^+_{II} cations and experienced by each $(WO_3)_2$ dimer will serve to (i) deplete the $(WO_3)_2$ of valence electron density (ii) weaken skeletal W-O bonds, (iii) destabilize the $O^{-II}(2p\pi)$ and stabilize the $W^{VI}(5d)$ MVB and MCB respectively, with a concomitant decrease in the band-gap (LMCT) energy, Figure 7. Because of the variation in population of, and distance between M^+_{II} cations, one does not expect the cation dependence of the miniband gap energy to be a straightforward function of ionic potential across the M = H, Li, Na, K, Rb, Cs series. Thus amonotonicity in E_g for $Li_{56}Y$ and $Na_{56}Y$ might relate to the known desire of Li^+_{II} to reside in the plane of oxygen 6-rings. Spatial constraints for $Rb_{56}Y$ and $Cs_{56}Y$ (90% M^+_{II}, M^+_{III}) could be the cause of their similar E_g values. The "special" position of $H_{56}Y$ in this series is probably related to the "dual" involvement of hydrogen-bonding (ZOH_α to terminal W=O) and protonation (ZOH_β to bridging W-O) found for $(WO_3)_2$ in $16(WO_3)$-$H_{56}Y$, (1). Rietveld PXRD structure refinements and EXAFS structure analyses are currently underway for the entire $n(WO_3)$-$M_{56}Y$ series in order to check the validity of the preliminary results and ideas presented above.

Summary

A simple chemical means of injecting electrons and holes into $n(WO_{3-x})$-$Na_{56}Y$ has been achieved ($0 \leqslant x \leqslant 1$). The method is applicable to isolated $(WO_3)_2$

dimers, coupled $(WO_3)_2$ dimers and a supralattice of coupled $\{(WO_3)_2\}_2$ dimers-of-dimers imbibed in the α-cage of the zeolite Y host lattice. An illustration of this concept is shown in Figure 8.

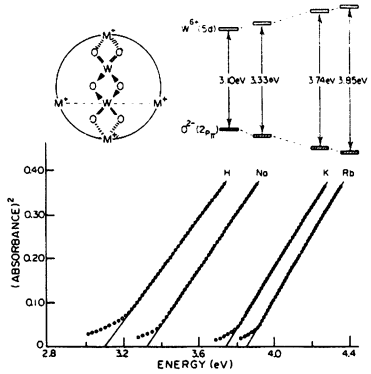

7. Experimental uv-visible absorption edges of a $16(WO_3)$-$M_{56}Y$ supralattice, where M = H, Na, K, Rb together with the best computer fit to the absorption index of an allowed-direct band gap transition, $\alpha^{da} = K(E - E_g)^{1/2}$. Inserts qualitatively illustrate the MVB/MCB energy levels for $16(WO_3)$-$M_{56}Y$.

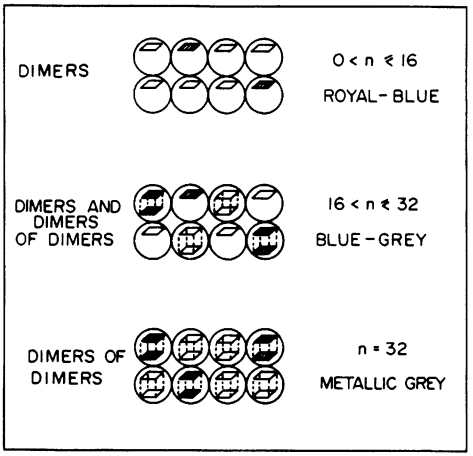

8. Intracavity and intercavity connectivity (coupling) in $n(WO_{3-x})$-$Na_{56}Y$ for $x < 0.5$.

Through alterations of the local electrostatic fields experienced by the $(WO_3)_2$ dimers, achieved by varying the ionic potential of constituent supercage cations, one is provided with a novel means of fine-tuning the miniband-gap of a tungsten(VI) oxide supralattice. Therefore cluster size, composition and intrinsic electrostatic field effects can be used to "chemically manipulate" (engineer) the doping and band architecture of organized assemblies of intrazeolite $(WO_3)_2$ dimers.

Acknowledgements

We wish to acknowledge (GAO, PMM) the Natural Sciences and Engineering Research Council (NSERC) of Canada's Operating and Strategic Grants Programmes for generous financial support of this work. Sö expresses his gratitude to the Middle East Technical University for granting him an extended leave of absence to conduct his research at the University of Toronto. K.M. and T.B. acknowledge partial funding for this work from the donors of the Petroleum Research Fund administered by the American Chemical Society. The operational funds for NSLS beamline X-11A are provided by DOE Grant Number DE-AS0580ER10742 (KM, TB) and NSERC (GAO). Supplies of high quality zeolites from Dr. Edith Flanigen at Union Carbide, Tarryton, N.Y. are gratefully appreciated. Dr. Heinz Robota of Allied Signal is acknowledged for his assistance with the collection and analysis of EXAFS data. The assistance of Dr. Andrew Holmes and Mr. Alex Kuperman with various aspects of this project are also most deeply appreciated.

References

1. G.A. Ozin and S. Özkar, J. Phys. Chem., 94, 7556(1990).
2. (a) G.A. Ozin, S. Özkar, K. Moller and T. Bein, J. Amer. Chem. Soc., 112, 9575(1990); (b) G.A. Ozin, S. Özkar and P.M. Macdonald, J. Phys. Chem., 94, 6939 (1990); (c) G.A. Ozin, S. Özkar, K. Moller and T. Bein, J. Phys. Chem., (in press).
3. G.M. Varga, E. Papaconstantinou and M.T. Pope, Inorg. Chem., 9, 662-667 (1970).
4. G.A. Ozin, S. Özkar, A. Malek, P.M. Macdonald, A. Pines, R. Jelinek, (work in progress).
5. H. Robota (private communication).